coatings

MDPI

Article

Evaluation in Real Conditions of New Anticorrosive Formulations Based on Polyphenols from Natural Sources and Encapsulated Nanoparticles

Jesús Ramírez [1], Andrés Díaz-Gómez [1], Luis Felipe Montoya [2], Saireddy Shiva Samhitha [1], David Rojas [1,*], Ángelo Oñate [1], Andrés Felipe Jaramillo [3,4] and Manuel Francisco Melendrez [1,5,*]

[1] Interdisciplinary Group of Applied Nanotechnology (GINA), Hybrid Materials Laboratory (HML), Department of Materials Engineering (DIMAT), Faculty of Engineering, University of Concepcion, 270 Edmundo Larenas, Box 160-C, Concepcion 4070409, Chile
[2] Department of Chemical Engineering, University of Concepción, Edificio Gustavo Pizarro Barrio Universitario S/N, Concepcion 4070409, Chile
[3] Department of Mechanical Engineering, Universidad de La Frontera, 01145 Francisco Salazar, Temuco 4780000, Chile
[4] Departamento de Ingeniería Mecánica, Universidad de Córdoba, Cr 6 #76-103, Montería 230002, Colombia
[5] Unidad de Desarrollo Tecnológico, 2634 Av. Cordillera, Parque Industrial Coronel, Concepción 4191996, Chile
* Correspondence: davrojas@udec.cl (D.R.); mmelendrez@udec.cl (M.F.M.); Tel.: +56-41-2207170 (D.R.); +56-41-2203187 (M.F.M.)

Abstract: The objective of this study was to examine the combined protection effect of a two-layer system consisting of organic corrosion inhibitors (tannins derived from the bark of radiata pine) and anodic protection by means of the incorporation of zinc oxide nanoparticles modified superficially by chemical methods to improve the protection of metallic structures against corrosion. Film evaluations are performed in accordance with ISO and ASTM standards. This study also took into account the evaluation of the performance of two commercial coatings according to the scheme suggested by the supplier, in addition to the electrochemical impedance spectroscopy (EIS) characterizations at 0 h, 720 h of accelerated exposure, and 4 months of atmospheric exposure in a corrosive environment of classification C3. The results obtained indicated that the combination of tannins derived from pine bark and encapsulated zinc oxide nanoparticles is a viable alternative to commercial coatings with a higher concentration of synthetic compounds. Although the film properties decrease slightly, performance tests at different exposure times show that they can still be classified as high-performance coatings.

Keywords: atmospheric corrosion; corrosion protection; epoxy resin; tannins; ZnO nanoparticles

Citation: Ramírez, J.; Díaz-Gómez, A.; Montoya, L.F.; Samhitha, S.S.; Rojas, D.; Oñate, Á.; Jaramillo, A.F.; Melendrez, M.F. Evaluation in Real Conditions of New Anticorrosive Formulations Based on Polyphenols from Natural Sources and Encapsulated Nanoparticles. *Coatings* **2023**, *13*, 8. https://doi.org/10.3390/coatings13010008

Academic Editors: Sebastian Feliú, Jr., Federico R. García-Galván and Michele Ferrari

Received: 30 September 2022
Revised: 2 December 2022
Accepted: 12 December 2022
Published: 21 December 2022

1. Introduction

The behavior of metals and alloys is mostly determined by the local meteorological variables such as temperature, relative humidity, humidification time, acid rain, direction and speed of the winds, and solar radiation in addition to the present atmospheric pollutants (chlorides, sulfur dioxide, carbon dioxide, and nitrogen oxides) [1–4]. The application of international standards permits the categorization of the environment's abrasiveness, which permits the estimation of the material's degree of deterioration during engineering design. For a long time, scientists studying the subject of corrosion and the technicians responsible for the design of protection systems and the maintenance of metal structures exposed to the atmosphere have been in constant need of maps and a wide range of raw materials focused on meeting this need [5–7]. At the local level, Vera et al. [4,6] have joined efforts to create a map of atmospheric corrosion in Chile, a country characterized by a diversity of corrosion-prone climates, being coastal (chloride contamination), and its industrial areas, with pollution by sulfur dioxide (SO_2) gas, which causes acid rain in the

presence of moisture. The authors found in their studies that the corrosion rates at 3, 6, 9, and 12 months for carbon steel in 30 monitoring stations throughout Chile present different corrosion rates. In said study, it was possible to observe the use of regulations to classify corrosive environments, where C1 indicates areas with the lowest corrosion rate and C5 the areas with the highest aggressiveness.

The data presented above indicate that applied research in the anticorrosive protection of metallic materials is extremely important, especially as atmospheric pollution and the rate of corrosion increase over time [5]. Therefore, the sum of efforts to tackle a portion of the discussed challenge is replete with intellectual, technological, and economic benefits for nations that bet on these breakthroughs. Therefore, the protection of metallic materials against corrosion will always be a research niche and any technical advancement in this field will result in cost savings and the creation of more ecologically friendly products. When faced with this problem, there are various methods for protecting materials against corrosion. Nevertheless, it should be emphasized that any protection strategy tries to limit the pace of corrosion, as the natural cycle of material deterioration cannot be prevented [8,9]. The use of high purity materials, special heat treatments to homogenize solid solutions, such as stress relief, the presence of compounds in materials such as alloying agents, the addition of inhibitors in corrosive solutions to reduce their effect, cathodic protection, oversizing, and surface coatings such as paints, oxide layers, or metal coatings are among the existing methods [10–15].

To achieve protection against corrosion using coatings, it is necessary to have the correct formulation of paints in addition to an adequate application scheme. The latter consists of adding a series of successive layers of paint, since each layer has a specific function. The first layer, known as "primer", protects the substrate and improves the physical and chemical properties of subsequent layers. Thereafter, an anti-corrosion layer is applied to create a sacrificial coating, usually with a chemical component (anti-corrosion pigment). Finally, a "top coat" is applied, which creates a barrier against external corrosion. This research focuses on evaluating a two-layer anticorrosive protection scheme formulated from the incorporation of inhibitors extracted from natural sources and surface-modified zinc oxide nanoparticles [16]. With this, the aim is to develop a first layer that acts as a primer and anticorrosive and a second finishing layer with functional properties. The inhibitors used in these formulations as a novel alternative was extracted from the bark of Pinus radiata, which were incorporated into a formulation of a two-component primer (2 K) based on solvent (epoxy resin). The most important parameters in the formulations of coating are volumetric concentration of pigment (PVC) and the critical volumetric concentration of pigment (CPVC), which results in achieving the best properties required by the industry [17,18].

On the other hand, in addition to the pursuit for new organic inhibitors, a new concept of coating known as functional or intelligent coatings has lately emerged as one of the most promising advances in high-performance anti-corrosion systems for a wide range of industries. Thanks to advances in nanotechnology, with the synthesis of nanostructured materials, these coatings with functionalized fillers can be adapted to many applications. This enable the capability to perform well-defined functions such as hydrophobicity [19], thus creating enormous opportunities in the corrosion inhibition of metals and alloys. This new coating technology offers several benefits, including reduced maintenance costs and surface cleaning time [20]. There are numerous coating systems based on epoxy resins that contain metal oxide nanoparticles such as ZnO, TiO_2, and Fe_2O_3 that attribute better protection capabilities against corrosion due to their uniform distribution [21]. It is important to mention that the second layer of the protection scheme developed in this work complies with these functionalities and is achieved due to the incorporation of surface-modified zinc oxide nanoparticles.

From a technical-economic standpoint, paints are the most appropriate method for the protection of materials used in construction and industry, which is why almost 95% of companies use this system [22,23]. Studies conducted on large structures, particularly on

the hulls of ships and tanks in the oil industry, have determined that, in general, paints with both lower performance and lower costs require a surface preparation of no less than 20% of the total after the first year and that after four-to-five years it is necessary to reapply the entire protection scheme [18]. To comprehend the processes associated with the degradation of coating and to propose the protection mechanism of the said coating in contrast to steel causes this kind of research to be vital for users who want to protect metal structures or scientists who develop new coatings and/or materials.

In this same order of ideas, it is vital to comprehend that corrosion is a process that is dependent on exposure time; several studies have combined the use of periodic electrochemical tests and atmospheric exposure [19,22,23]. Rosales et al. conducted one of these studies, which consisted of subjecting coating formulations to three distinct marine air conditions and assessing their performance using electrochemical impedance spectroscopy (EIS) after varied exposure times [24]. The coating formulations applied to the steel substrate that consisted of a paint system based on galvanized Zn and 55% Al–43.5% Zn–1.5, which were exhibited in Jubany, Argentina (marine-polar), Punta del Este, Uruguay (marine), and La Voz, Venezuela (marine-desert). These experimental results demonstrated that the coating strength values obtained by EIS correlated well with the characteristics of the coatings observed during visual inspection. The lowest values of coating resistance coincided with the presence of large rust stains on the samples, confirming their poor barrier and anticorrosive properties under the experimental conditions [24].

It is evident that the use of periodic electrochemical testing of specimens at atmospheric exposure sites can provide useful information on coating protection against the corrosion of the material to be protected. To better comprehend the mechanics of corrosion and the protection offered by the various coating systems, it is necessary to distinguish between the different forms of protection they provide [25]. The main type of protection is the barrier against the entry of water and ions. This type of protection works by effectively sealing the substrate from the corrosive environment and can be examined by analyzing intact areas of coating samples. However, barrier protection is compromised in areas of a coating that contain a defect. Protection in defective areas can be provided by sacrificial coatings that generate an inhibitory effect in which the paint layer preferentially corrodes, thus forming an oxide film by reacting with the substrate, passivating the surface [26].

Based on the previous studies and the problems raised, this study formulated and evaluated a two-layer anticorrosive protection scheme with organic inhibitors (Pinus radiata tannin) and encapsulated zinc oxide nanoparticles. The ZnO-NPs used were synthesized by the physical method named continuous arc discharge in controlled atmosphere (DARC-AC) and modified by chemical methods [27]. The formulation of the coatings was accomplished utilizing fillers and additives and incorporating tannin as an organic inhibitor and modified ZnO-NPs as an inorganic inhibitor and as a material that improves protection against corrosion. For the characterization, electrochemical impedance spectroscopy (EIS) was used for the study of anticorrosive properties and standardized tests for the evaluation of mechanical properties of films. The plates painted with the formulated scheme were compared with the performance of two commercial schemes, exposing the samples to different time frames and environmental atmospheric conditions of the central-southern zone of Chile.

2. Materials and Methods

The following raw materials were used in the synthesis, functionalization, and encapsulation of zinc oxide nanoparticles (ZnO-NPs): 2 mm diameter Zn wires distributed by Sulzer (Winterthur, Switzerland), 3-aminopropyltriethoxysilane (APTES), toluene and ethanol, organic monomer, and analytical grade potassium peroxodisulfate supplied by Sigma and Aldrich. For the formulation of the anticorrosive coating, radiata pine tannins, solvent-based epoxy resin derived from bisphenol A, amide-based hardener, acrylic diluent, titanium dioxide grade R1, mica, calcined kaolin, and pyrogenic silica (Aerosil® 200) were used, followed by a dispersing agent (Antiterra® u) and a film leveling agent derived from

silicon. For the finishing coat, urethane-type polymers (Polyol LHT 112) were used and diphenylmethane di-isocyanate as a crosslinking agent, polyurethane thinner as a solvent, leveling additives (BYK® 333 and BYK® 425), moisture sequestrants (Purmol 3A), and dispersing agent (Antiterra® u).

2.1. Encapsulation of Zinc Oxide Nanoparticles

The processes of synthesis [19], functionalization, and characterization of ZnO-NPs were carried out by the research group (GINA). The encapsulation process consisted of the coupling of functionalized ZnO-NPs by emulsion polymerization using styrene as the organic monomer and potassium peroxydisulfate (KPS) as the reaction initiator. The ZnO-NPs were loaded in a 2 L flask with 40 mL of styrene and 400 mg of KPS in 1200 mL of distilled water. Subsequently, the mixture was sonicated for 30 min and subjected to mechanical stirring for 8 h at 80 °C, adding 25 mL of the initiator every 30 min. After this process, the particles were filtered, washed (toluene), and dried in an oven at 80 °C. The microstructural characterization of the ZnO-NPs was performed using X-ray diffraction (XRD) and transmission electron microscopy (TEM), while the characterizations of the encapsulated ZnO-NPs was performed using Fourier-Transform Infrared Spectroscopy [20].

2.2. Formulation and Application of Primer-Anticorrosive Coating and Top Coat

The primer-anticorrosive coating was manufactured using a high-speed disperser and a basket mill. Before the addition of the raw materials in the disperser, the encapsulated ZnO-NPs were ground with zirconium balls in a planetary ball mill (RETSH brand) for 1 h and sieved with a ϕ203 sieve and 38 µm aperture. Following this step, the components shown in Table 1 were mixed in a high-speed disperser and dispersed at speeds from 900 to 1200 rpm. Subsequently, the mixture was transferred to a basket mill with a cooling system, which carried out the grinding process at a speed of 1400. Once the grinding was finished, the particle size was verified using the grindometer according to the ASTM D-333 standard, reaching a value of 5.5 Hegman.

Table 1. Main components of the primer and top coat.

Primer Components	Percentages (%)	Components of Top Coat	Percentages (%)
Resin	35.22	Poliol 112	30.11
Tannins	0.1–5	BYK 333	0.44
Titanium Dioxide	10.62	BYK 425	12.00
Calcium Kaolin	15.60	Additives (BYK 333, Purmol 333, Antiterra)	0.94
Mica Muscovite	17.80	ZnO-NPs	3.00
Additives	0.42	Thinner	38.40
ZnO-NPs	3.00	Crosslinking	30.11
Crosslinking	8.8	-	-
Thinner	Adjustment up to 100%	-	-

Regarding the formulation of the top coat layer, the same methodology was carried out. However, the components are those shown in Table 1. The surface preparation of the metallic substrate (ASTM A36 Steel) was carried out according to the standards established by the SSPC (Steel Structures Painting Council, Pittsburgh, PA, USA), applying sections SP1 and SP5. The formulated coatings were applied to the metal surface by means of an air gun with a wet thickness between 150 and 200 µm. The coating application process was divided into two steps: (1) application of the primer-anticorrosive and (2) application of the top coat; a drying time of one week between the coats was allowed. In order to compare the mechanical properties and corrosion resistance in the formulated coating, commercial solvent-based primer anticorrosive paints and a top coat were used. They

were applied according to the methodology explained above. Once the application of the coatings was finished, the following nomenclature was established for the identification of the specimens: primer-top coat formulation (PT-ZnO NPs), commercial polyurethane paint (PU, supplied by Delfin coatings), and commercial transurethane paint (TE, supplied by Transocean coatings).

2.3. Meteorological and Meteorochemical Characterization of the Monitoring Station

The characterization of the monitoring station was carried out in the Maritime Government of Talcahuano, Chile (Latitude 36.71 S and Longitude 73.11 W) at 3 m above sea level and a 27 m linear distance. An atmospheric corrosion monitoring frame was installed with 12 carbon steel samples coated with the coating schemes to be evaluated. The dimensions of the samples studied were $10 \times 10 \times 0.2$ cm^3 and they were placed in the rack with an inclination of 45° with respect to the horizontal axis, which was separated with Teflon insulators to avoid galvanic corrosion of the samples as indicated by the ISO 9223 and ISO 9226 standards. Figure 1 shows the location of the monitoring frame. Additionally, devices were installed to evaluate the content of the meteorochemical pollutants such as chloride and sulfur dioxide present in the environment according to the ISO 9225 standard. The percentage of chlorides (Cl^-) was obtained with the wet candle method and the percentage of SO_2 by the lead peroxide candle method. Both the results are expressed in mg m^{-2} day^{-1} of each compound, respectively. Likewise, a thermohygrograph was used to measure the temperature and relative humidity (RH) to determine the time of wetting (TOW), according to ISO 9225 [6].

Figure 1. Location of the monitoring station in Maritime Government of Talcahuano, Chile.

2.4. Evaluation of Functional Properties in Accelerated Tests

The functional properties of the film (mechanical and corrosion resistance) were evaluated by means of accelerated tests on the different coating schemes (PT-ZnO NPs, PU, and TE). The accelerated conditions were simulated through prohesion tests (exposure to a weathering chamber and salt spray). The evaluation consists of a combination of

two tests: the salt spray corrosion test (ASTM G85) and the weathering test using high humidity and UV radiation (ASTM G154). The trials alternate between cycles A and B each week until 720 h are completed. Table 2 shows the exposure conditions for each cycle. Additionally, the coatings were exposed at the monitoring station in the Maritime Government of Talcahuano, located in the city of Concepción, Chile, at 3 m above sea level. The functional properties were evaluated in accelerated tests at 0 and 720 h, and in the field at 0 and 4 months of exposure (ASTM D5894-16).

Table 2. Exposure conditions of each cycle of accelerated tests.

Accelerated Tests	Cycle A (Salt Fog Chamber)	Cycle B (Weathering Chamber)
Conditions of each test	1 h salt spray at 25 °C	4 h UV exposure, lamps UVA 340, 60 °C
	1 h drying at 35 °C	4 h condensation at T 50 °C

2.4.1. Film Properties

The film properties were evaluated by visual inspection through blistering, rust formation, cracking, and chalking according to the ISO 4628 standard. In addition, the wet (ASTM D4414-95) and dry (ASTM B499) thicknesses were determined.

2.4.2. Mechanical Properties

The mechanical properties of the evaluated schemes were carried out according to standard tests of the appropriate ASTM and ISO standards in different exposure media (accelerated and field tests). The coating thickness was determined (ASTM D 6132) using an Elcometer 456 m. The adhesion test standard ASTM D-4541, using the PosiTest AT-A equipment, with aluminum dollys with a diameter of 20 mm. The flexibility test was conducted (ASTM D 522-08) using a Neurtek Mandrel Bend Tester. The deep drawing tests were carried out under the ISO 1520 standard using a Neurtek CT15 stuffer and resistance to abrasion (ASTM D 4060) using a Taber Abraser model 5131, with a load of 1000 g and abrasion wheels type CS-17.

2.4.3. Resistance to Corrosion

The anticorrosive properties of the coating were evaluated using the electrochemical impedance spectroscopy (EIS) technique in both media (accelerated and field) (ASTM G102). A cell with 3 electrodes was used: a working electrode (coated plate), a saturated calomel (KCl) reference electrode, and an auxiliary graphite rod electrode. The electrodes were immersed in a 0.1 M Na_2SO_4 solution and connected to a VersaSTAT 3 potentiostat (Princeton Application Research) following the STP18062S standard. An open circuit potential of 900 s was applied and, subsequently, the EIS measurement was performed in a frequency range between 50,000 Hz and 0.1 Hz and 15 mV.

3. Results and Discussions

3.1. Synthesis, Functionalization, and Encapsulation of ZnO Nanoparticles

The synthesis of the ZnO nanoparticles obtained using the DARC-AC equipment was characterized by TEM and XRD. The X-ray diffraction results in ZnO-NPs revealed intense and well-defined peaks, confirming the presence of wurzite, with the main diffracted planes being (100), (002), (101), (102), (110), (103), (112), (201) (112), and (004) (see Figure 2a). In addition, the presence of other phases from the synthesis of the nanoparticles was not detected. This is to be expected given that the applied methodology only uses a precursor wire of metallic zinc and oxygen gas, both of high purity. On the other hand, when studying the ZnO-NPs by TEM, irregular rod shapes and an average particle size distribution of 56 nm were observed, as shown in Figure 2b,c. In this regard, when compared to other nanoparticle manufacturing procedures, the average particle size achieved is within the specified values and fulfills the high purity criteria [28–30].

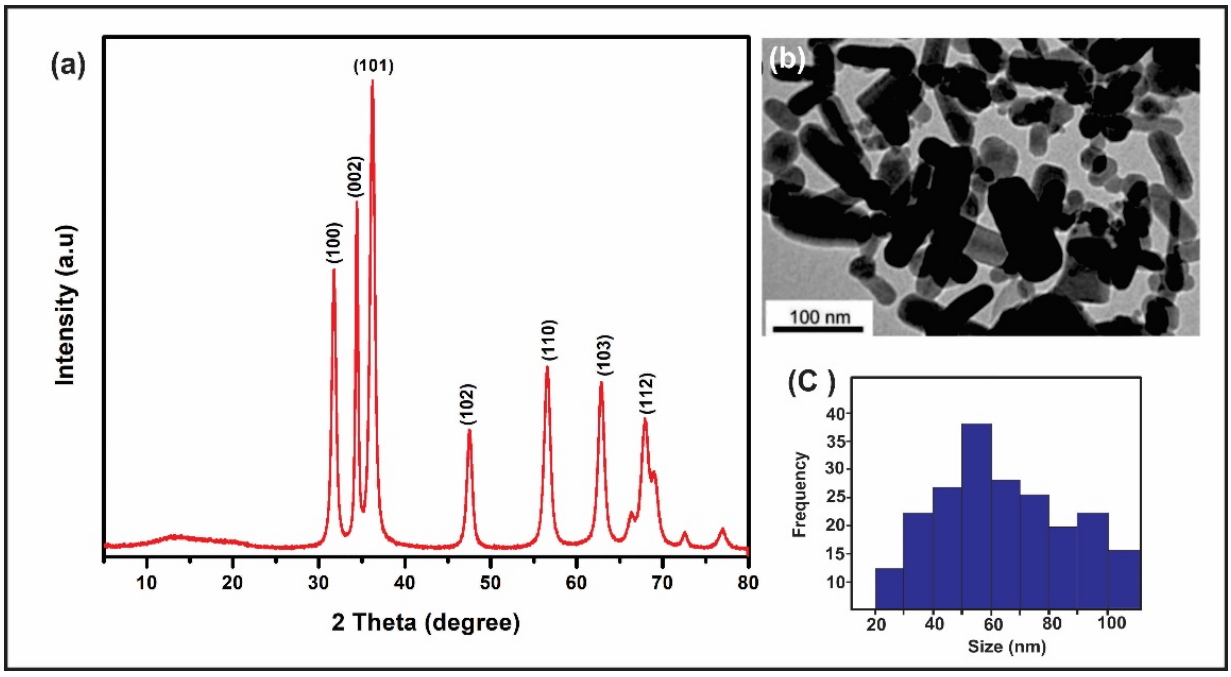

Figure 2. Characterization of ZnO-NPs: (**a**) XRD, (**b**) TEM, and (**c**) ZnO-NPs size.

Regarding the encapsulation process of ZnO-NPs with styrene studied by FT-IR. The IR spectrum in Figure 3a shows the characteristic curves of the main raw materials and encapsulation process: styrene (St), ZnO-NPs-St, and ZnO-NPs. The characteristic signals of styrene, mainly the signals at 3020–3100 cm^{-1}, are associated with the C-H stretching band, in addition to the C-H bending bands at 1487–1432 cm^{-1}, and finally the absorption bands between 1630 and 1500 cm^{-1}, corresponding to the vibration of the aromatic C=C bond. In the ZnO-NPs, signals at 873 cm^{-1} and 572 cm^{-1} are observed, which are characteristic of the vibration of the Zn-O bond, and a signal at 3413 cm^{-1} associated with the characteristic absorption of hydroxyl groups. The ZnO-NPs encapsulated with styrene can be detailed by the disappearance of the signal at 1630 cm^{-1} corresponding to the stretching vibration of the C=C double bond of the styrene group, which confirms the polymerization in the respective encapsulation conditions. The signals at 1483, 752, and 711 cm^{-1} are attributed to the absorptions in the phenyl groups, confirming the existence of polystyrene on the surface of the nanoparticles. On the other hand, the effective coupling of styrene molecules to the surface of ZnO-NPs was studied by TGA. Figure 3b shows a considerable loss of mass of the encapsulated nanoparticles with respect to the unmodified ZnO-NPs with values of 2.54% and 2.84%, respectively. The weight loss corresponding to temperatures below 350 °C is attributed to styrene. The thermal degradation of polystyrene occurs in the temperature range from 350 °C to 450 °C. Finally, at 450 °C, it corresponds to ZnO losses. The results obtained confirm the coupling of the ZnO-NPs by encapsulation with styrene [28]. In addition, the synthesis, functionalization, and encapsulation meet high purity standards compared to other nanoparticle production processes. In this sense, ZnO-NPs-St can be added to new anticorrosive formulations.

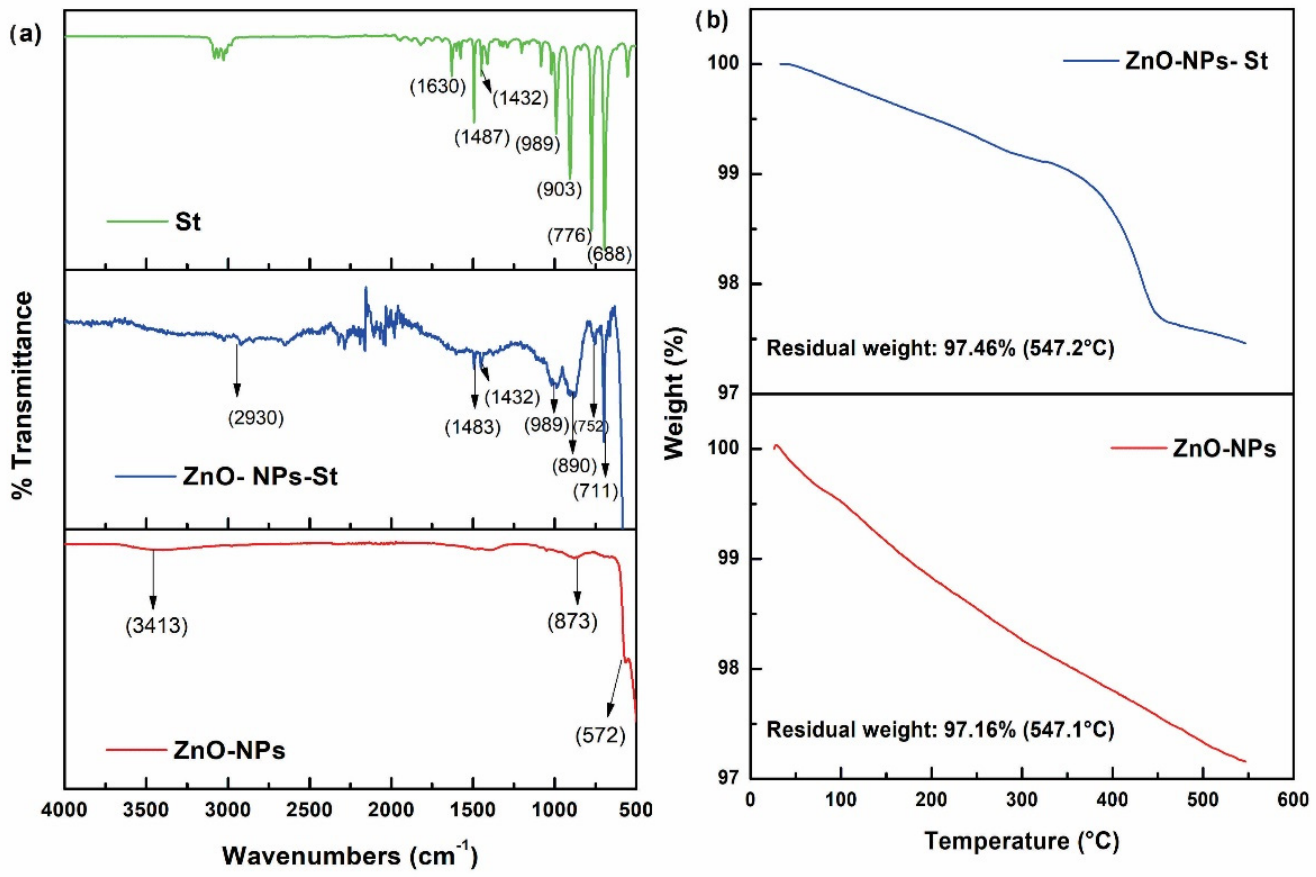

Figure 3. Fourier-Transform Infrared Spectroscopy: (**a**) St, ZnO-NPs-St, and ZnO–NPs. (**b**) Thermogravimetric analysis of ZnO-NPs and ZnO-NPs-St.

3.2. Meteorological and Meteorochemical Characterization of the Monitoring Station

The meteorological characterization was evaluated between April 2018 and March 2019, reporting relative humidity, temperature, precipitation, and wind speed. Figure 4 shows a summary of the meteorological variables measured at the Talcahuano Maritime Government station in the four seasons of the year. The relative humidity remains at approximate values of 80% throughout the year. This variable is crucial in determining atmospheric corrosion (See Figure 4a). At a relative humidity value of below 60–70%, there is no appreciable film of electrolyte on the metal and corrosion is negligible. However, in this evaluation study, the humidity is close to 80%, so its effect on the coatings will depend on other factors such as the soluble constituents (sulfur dioxide and chlorides), which enhance the corrosive process. The temperature and precipitation levels are consistent with the seasons of the year, with an increase in temperature observed in the spring and summer seasons and an increase in precipitation observed in the autumn and winter seasons (see Figure 4b). On the other hand, the wind speeds, according to the results shown, are high in the autumn and winter periods; therefore, it is to be expected that during these seasons there is a more erosive environment in the coatings. Lastly, the average solar radiation was 1454 kW/m^2 in areas near the station. This last variable is of great interest since it affects the properties of the coatings, causing their progressive deterioration. Solar radiation has the main effect of changing the color tones and brightness of the coatings, which will be developed in greater depth in the discussion of film properties. The results obtained for relative humidity and temperature allowed the determination of the wetting time (TOW). The sum of the partial wetting times constitutes the so-called time of wetting, during which corrosion is possible. To calculate the wetting time, RH $\geq$ 80% and temperature above 0 °C were used as the critical value, as indicated by ISO 9223 [6,31–33].

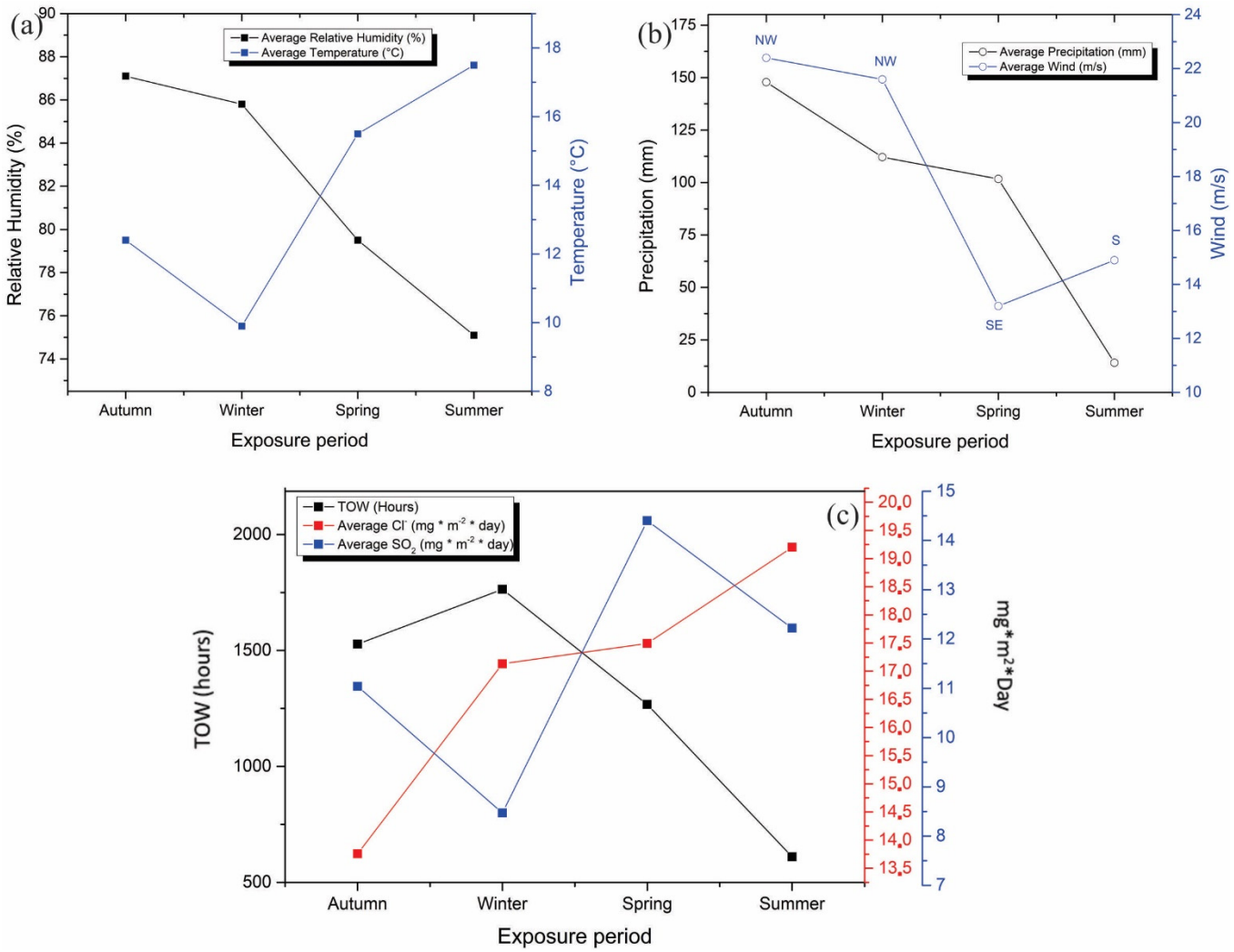

Figure 4. Meteorological variables measured at the Talcahuano Maritime Government station: (**a**) relative humidity and temperature, (**b**) Precipitation and wind, and (**c**) Meteorochemical characterization (TOW, SO_2, Cl^-).

The meteorochemical characterization was carried out on a quarterly basis, recording the deposition rates of the main corrosive agents, sulfur dioxide, and chlorides, based on ISO 9225 standards. The results obtained are shown in Figure 5. The atmospheric chloride content was determined using the humidity candle methodology, followed by a mercurimetric titration in the presence of diphenylcarbazone and bromophenol blue indicators. The results of the deposition of environmental chlorides were higher in the spring and winter seasons, with average values of 19.2 and 16.9 mg Cl^-/m^2 day, characterizing the depositions as S1 ($33 < S \leq 60$) according to the ISO 9223 standard (Figure 4c). The sulfur dioxide content presents similar results to the chloride content, obtaining the highest concentrations of SO_2 in spring and winter with average values of 14.44 and an average of 11.53 mg SO_2/m^2/day, categorizing the monitoring station as P1 ($10 < Pd \leq 35$) according to the ISO 9223 standard. According to the results of TOW, Cl^-, and SO_2 content, the environmental aggressiveness in the Talcahuano Maritime Government station is classified as category C3, an atmosphere of medium aggressiveness [31,34–36].

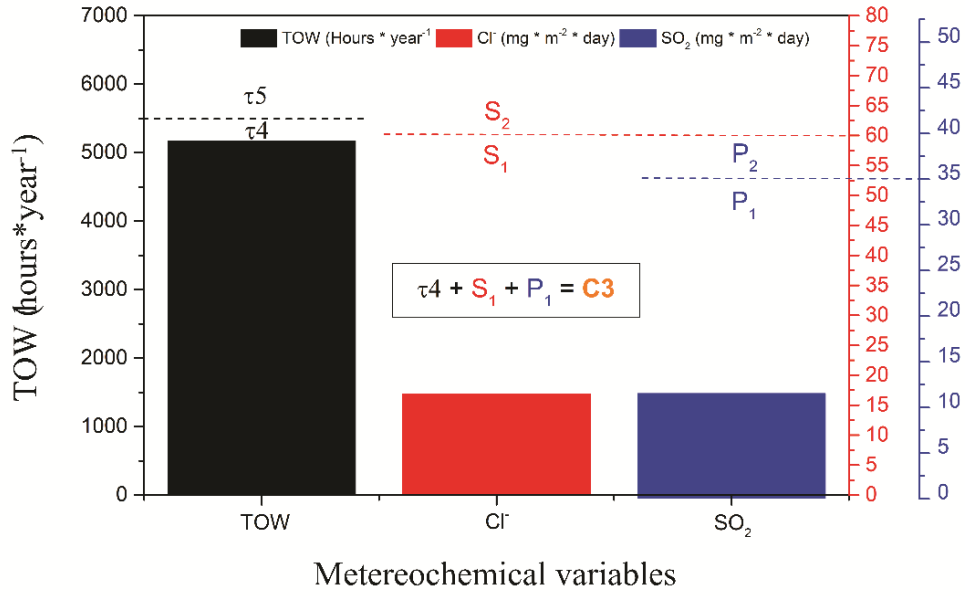

Figure 5. Meteorological variables measured at the Talcahuano Maritime Government station.

3.3. Evaluation of the Functional Properties of the Coating in the Accelerated Corrosion Chamber and in the Field

3.3.1. Film Properties

The optimum wet thickness for application in the coatings is 200 microns for the layer primer and the top coat layer in the order of 100 microns. Subsequently, the drying film presented a thickness of between 170 and 250 microns for a time of 0 h in PT-ZnO NPs, PU, and TE. At 720 h of exposure, there is a decrease in the thickness of the different coatings evaluated, with TE being the most affected coating compared to PT-ZnO NPs and PU. The thickness losses are attributed to the aggressive conditions of UV exposure cycles, spraying, condensation, and salt spray, which degrade the top layer. Figure 6 shows the thicknesses at 0 and 720 h in the evaluated coatings. To complement the description of the film properties, the coatings were inspected at 0 and 720 h of exposure according to ISO 4628.

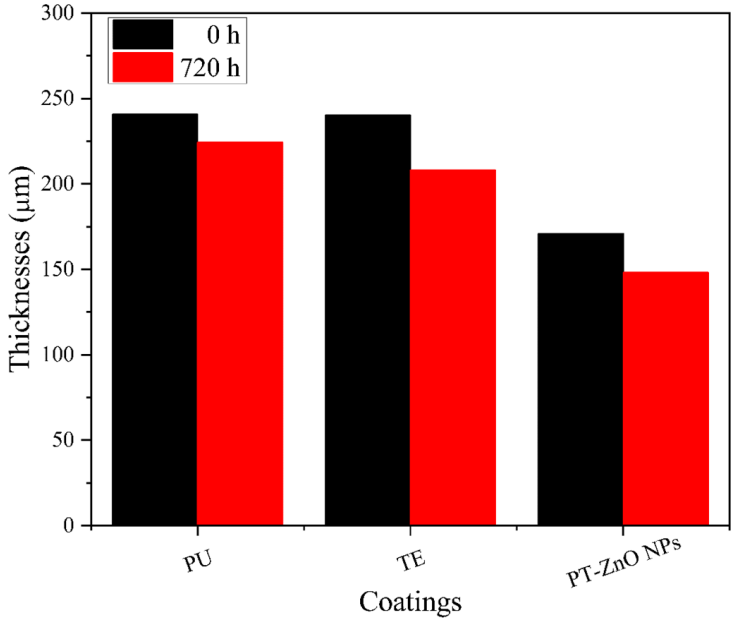

Figure 6. Coating thicknesses at 0 and 720 h of exposure.

The results at the time of 0 h did not present any irregularity on the surface of the coatings evaluated, while at 720 h of exposure they observed a loss of brightness and color change. The TE coating presented adhesion loss, 2S2 blistering, and 3S2b delamination, while the PT-ZnO NPs and PU coatings did not present any type of failure according to ISO 4628 (see Figure 7).

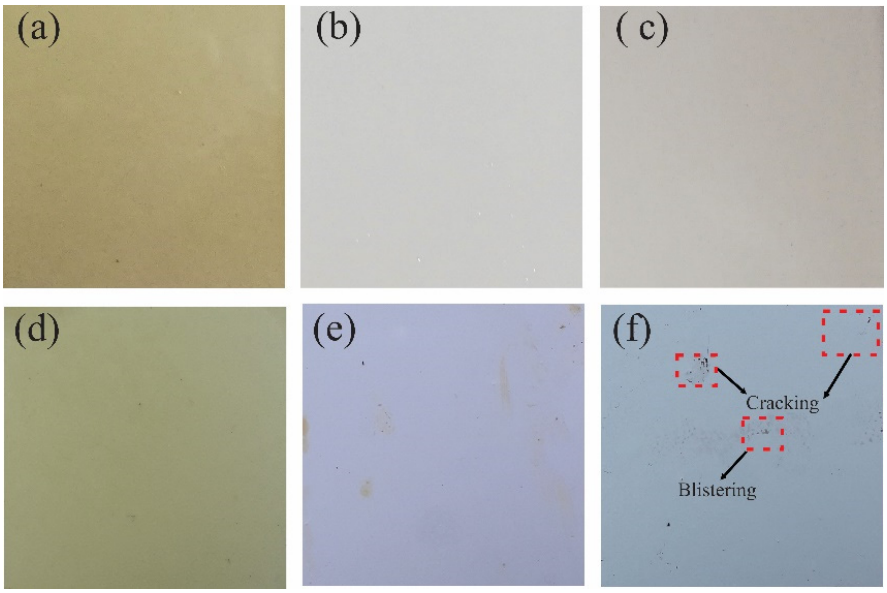

Figure 7. Visual inspection at 720 h of exposure in accelerated corrosion chamber: (**a**) PT-ZnO NPs 0 h, (**b**) PU 0 h, (**c**) TE 0 h, (**d**) PT-ZnO NPs 720 h, (**e**) PU 720 h, and (**f**) TE 720 h.

While the coatings were exposed to field tests, the results showed that at 0 days of time, there was no irregularity on the surface of the coatings evaluated, while at six months of exposure, loss of brightness and color change were shown. Changes in brightness and color are associated with factors such as ultraviolet radiation, precipitation, and wind, among others. In addition, the coatings exposed in field tests did not present loss of adhesion, blistering, delamination, or other types of failure according to ISO 4628. Figure 8 shows the visual inspection after 6 months of exposure in the field [36–39].

3.3.2. Mechanical Properties

The mechanical properties of the coatings were characterized at 0 h and 720 h using adhesion, impact resistance, flexibility, and abrasion tests. The adhesion was evaluated in accordance with the ASTM D4541 standard by applying the tensile test in triplicate using the PosiTes AT-A equipment. The force exerted per unit area on the specimens subjected to cyclic weathering tests in the salt spray chamber was determined. The acquired results are reported in Table 3. At 0 h, the PT-ZnO NPs coating had better adhesion than the PU and TE coatings, with values of 24.00, 18.15, and 5.12 MPa, respectively. Except for the TE scheme, which exhibited poor adhesion to the substrate, this behavior implies good adhesion between layers [17]. Regarding the type of failure presented on the layers, it was of the primer/top coat cohesive type in the evaluated coatings. After 720 h of exposure of the coatings, a decrease in or loss of adherence was observed as a consequence of the permeation of chlorides and the presence of moisture toward the substrate. In the PT-ZnO NPs and PU coatings, where adhesion decreased at values of 12.28 and 12.08 MPa, this loss of adhesion was more pronounced than in the TE coating, where adhesion decreased at a value of 4.55 MPa. This study indicates that TE exhibited superior adherence. Observing the type of failure, however, reveals the contrary, as there is a rupture between the primer and top layers. In this regard, the PT-ZnO NPs coatings exhibited outstanding interlayer adhesion.

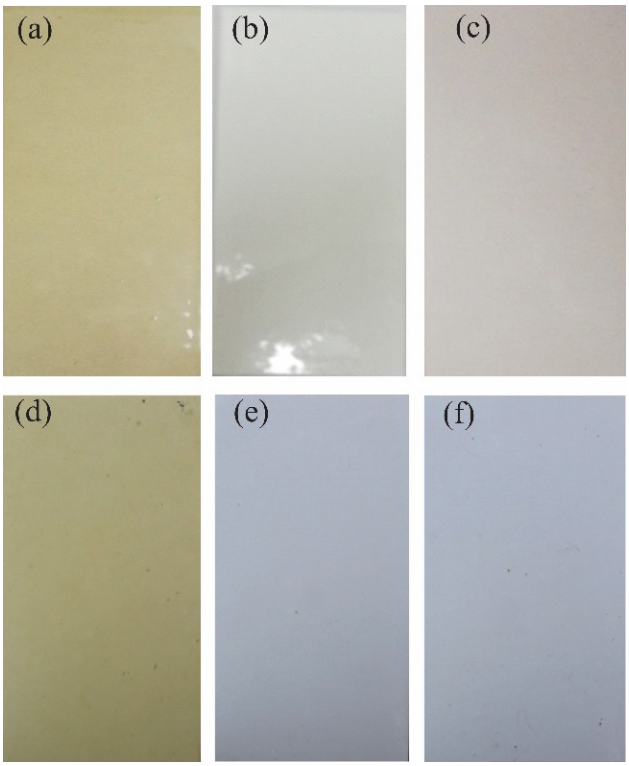

Figure 8. Visual inspection after 6 months of exposure in the field: (**a**) PT-ZnO NPs 0 h, (**b**) PU 0 h, (**c**) TE 0 h, (**d**) PT-ZnO NPs months, (**e**) PU months, and (**f**) TE 6 months.

Table 3. Type of failure in the coatings evaluated in the adhesion test.

Coatings	**Failure**	
Time (h)	0	720
PT-ZnO NPs	Cohesive	Adhesive Primer/Substrate
PU	Adhesive	Cohesive/Primer
TE	Adhesive	Adhesive Primer/top

Regarding the abrasion resistance tests, the results obtained at 0 and 720 h are shown in Figure 9a. The greatest losses at time 0 h correspond to the TE scheme compared to PT-ZnO NPs and PU, with values of 271.30, 92.40, and 91.60 mg, respectively. After 720 h of exposure to the accelerated chamber, there is an increase in coating losses, maintaining the highest losses in the TE scheme compared to PT-ZnO NPs and PU, with values of 338.10, 297.30, and 171.40 mg, respectively. The formulated PT-ZnO NPs coating presented abrasion losses not so far from the commercial coatings. This is possibly because the experimental system has lower thicknesses than the commercial schemes, which in turn is a good characteristic since if the thicknesses were close. However, if the thicknesses close to the commercial coatings are increased, a higher resistance would be expected for the PT-ZnO NPs followed by excellent mechanical properties. Likewise, the increase in losses in the evaluated schemes is attributed to the exposure medium, such as ultraviolet radiation, humidity, and chloride permeability. In this sense, the ultraviolet radiation directly affects the top coat layer, deteriorating its barrier properties against the aggressive medium of humidity and permeability. It is important to note that none of the coating schemes met the minimum wear loss (84 mg) expressed by the ASTM D4060 standard [21,40,41].

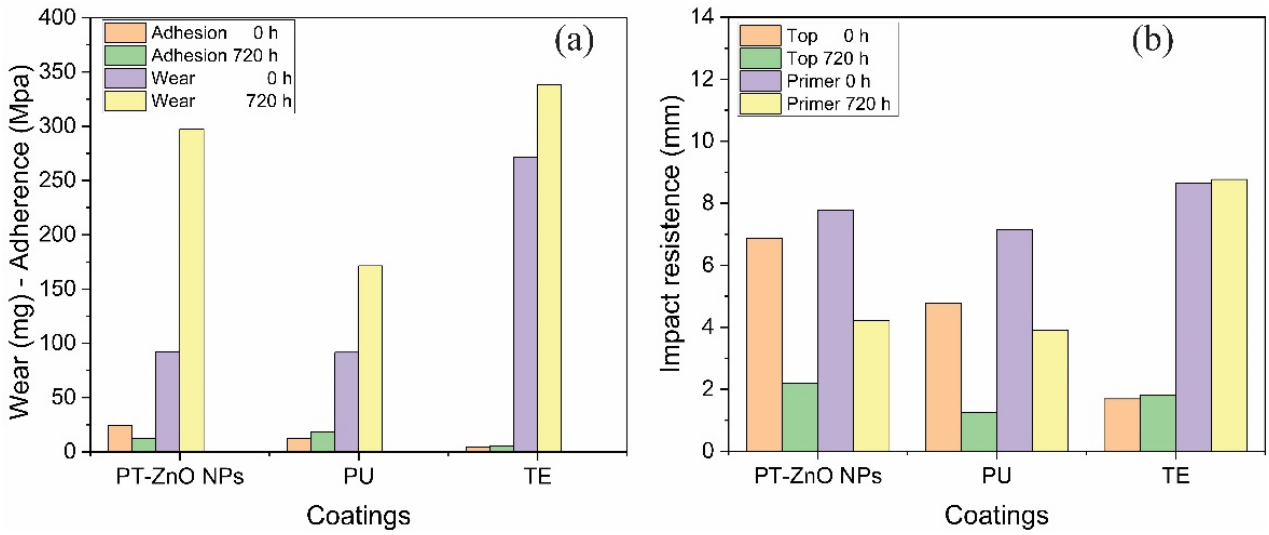

Figure 9. Mechanical properties for PT-ZnO NPs, PU, and TE: (**a**) wear and adhesion at 0 and 720 h of exposure; (**b**) impact resistance 0 and 720 h of exposure.

The characterization of the impact resistance on the coating was considered with the detachment between layers and from the substrate, for which the rupture measurements in the top and primer layers were reported. For time 0 h, it was observed that the highest resistance to the advance of the indenter in the top layer corresponds to the PT-ZnO NPs coating compared to TE and PU, with values of 6.86, 1.69, and 4.78 mm, respectively. While in the primer layer, there is a similar behavior in the advance of the indenter. After 720 h of exposure, a decrease in impact resistance was obtained in the top and primer layers in all the schemes evaluated. The decrease in impact resistance was greater in the commercial TE and PU coatings compared to PT-ZnO NPs. The interlayer properties of the PT-ZnO NPs coating were very good, which agrees with the abrasion and adhesion tests. However, the PT-ZnO NPs coating had a decrease of approximately 60% of its initial resistance. This decrease may be the product of the effect caused by the accelerated corrosion test. Figure 9b shows the impact resistance results of the coatings.

In the flexibility tests for the coatings, they were carried out with cylindrical mandrels of different diameters (10″, 5″, and 2″). The test ends with the detection of cracks visible to the naked eye in the coating. The results obtained at 0 and 720 h of exposure are shown in Table 4. For the initial evaluation (0 h), the best behavior was shown in the PT-ZnO NPs coating, in which it did not exhibit layer rupture when folded at 180° to the smallest mandrel (2″) compared to PU and TE, with breaks at 5″ and 10″, respectively [42,43].

Table 4. Results of the flexibility tests on the coatings.

	Flexibility					
Time (h)	**0**			**720**		
Coatings	**Diameter**			**Diameter**		
	10″	**5″**	**2″**	**10″**	**5″**	**2″**
PT-ZnO NPs	Pass	Pass	Pass	Pass	Pass	Fail
PU	Pass	Pass	Fail	Fail	-	-
TE	Pass	Fail	Fail	Fail	-	-

After the coatings are exposed to 720 h of (Weathering Chamber–Saline Fog Chamber), there is a loss of flexibility properties. When observing the breaks between layers in the commercial coatings (PU and TE) on mandrels with a larger diameter (10″), the PT-ZnO NPs is more resistant with a value of 5″. Figure 10 shows the specimens after the

flexibility and abrasion tests. These results are consistent with the adhesion, abrasion, and impact resistance tests, in which it was observed that the commercial TE coating has low mechanical properties compared to the formulated commercial coating and the commercial PU coating. Likewise, the results of the mechanical properties confirm that the formulated PT-ZnO NPs coating has similar or superior properties to the commercial coatings (PU and TE) with an exception in impact resistance in comparison with TE [26,29,44].

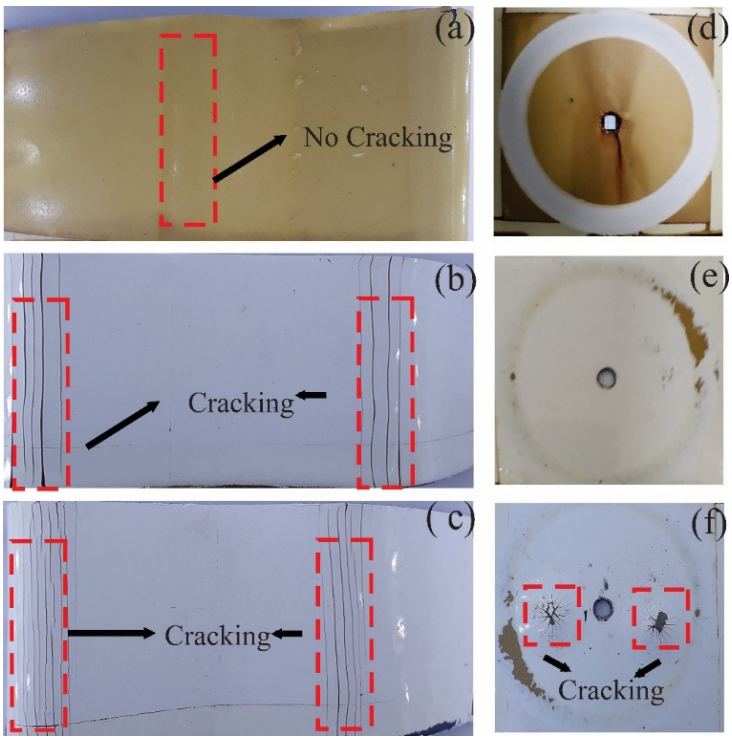

Figure 10. Flexibility and abrasion tests after 720 h of exposure. (**a**) PT-ZnO NPs flexibility, (**b**) PU flexibility, (**c**) TE flexibility, (**d**) PT-ZnO NPs abrasion, (**e**) PU abrasion, and (**f**) TE abrasion.

3.3.3. Evaluation of Anticorrosive Properties

Electrochemical impedance spectroscopy (EIS) analysis has been conducted on PT-ZnO NPs, PU, and TE coatings on steel in an accelerated chamber and the relative corrosion resistance of field tests were evaluated. EIS is well-known for the evaluation of coatings on metallic substrates as it allows the detection of the corrosive process from the initial stage prior to the visual degradation of the coating. The irreversible failure of the coating is detected when the low-frequency impedance modulus is matching with the resistance of the bare metal substrate measured in immersion [29,45,46]. In addition, it provides detailed information on the electrochemical behavior of the interface generated by exposing the coated sample to salt spray and field tests. The EIS results were plotted in typical diagrams such as: Nyquist or Bode. The Nyquist diagram is characterized by a semicircle offset from the origin of the complex plane that can be in a quantity equal to the ohmic resistance of the system (resistance of the solution). The diameter of the curves is considered as the charge transfer resistance (R_{ct}) and is inversely proportional to the electron transfer rate constant for a single time constant electrochemical interface. The diameter of the curves is considered as the charge transfer resistance (R_{ct}) and is inversely proportional to the electron transfer rate constant, for a single-time constant electrochemical interface. However, the presence of more than one semicircle diameter on the Nyquist plots may represent solution resistance, charge transfer resistance, and coating ohmic resistance, respectively. While in the Bode plot, two graphs are obtained, the first as a function of the modulus [Z] and the frequency and the second is referred to as phase angle θ and frequency. In this investigation, the results of the Nyquist and Bode graphs were considered

for the determination of the different resistances present in the behavior of the coatings. The impedance modulus [Z] at 0.1 Hz was used as an indicator of the corrosion resistance organic coating barrier properties corrosion.

Coating Exposed to Prohesion Tests (Exposure to a Weathering Chamber and Salt Spray)

Figure 11 shows the Nyquist and Bode diagrams of the impedance data of different coatings after prohesion tests. At 0 h of immersion, the Nyquist diagram of coatings present a high ohmic resistance with the formation of one incomplete resistive semicircle for PU, TU, and two semicircles in PT-ZnO NPs (Figure 11a). The modulus of the Bode plot at 0 h displays a straight line with a slope value close to −1 for PU, whereas for TE and PT-ZnO NPs there is a change in the slope at high and low frequencies (Figure 11b). The impedance modulus [Z] at 0.1 Hz exhibited very high values (>10^9 Ω cm^2) and the corresponding phase angle was close to 90 degree (Figure 11c). The impedance modulus [Z] at 0.1 Hz of coating with commercial PU, TE, and PT-ZnO NPs are 6.40 × 10^{10}, 8.98 × 10^9, and 2.51 × 10^9 Ω cm^2, respectively. This behavior at 0 h of exposure indicates a high resistivity to the permeability of the aggressive agent (saline mist) through the pores. The impedance modulus [Z] at 0.1 Hz value presented by the coatings is greater than 1 × 10^8 Ω cm^2, implying that there is an excellent protective layer of the metallic substrate against aggressive agents [47–49].

After 720 h of exposure to prohesion tests (saline mist and weathering), the Nyquist diagram of coatings shows a decrease in the diameter of the semicircle and the formation of one incomplete semicircle for PU and PT-ZnO NPs (Figure 11a). However, in TE coatings, the semicircle becomes almost complete during the exposure time. The reduction in the diameter of the semicircle indicates a decrease in the resistance to the exposure medium, which influences the increase in the capacitance of the coating which is observed in the protective performance of the coating. In Figure 11b, the Bode diagram log frequency versus the phase for the analyzed coatings, there exists one-time constants and the corresponding phase angle between 90 and 120 degrees. The modulus of the Bode plot exhibits a straight line with a slope value close to −1 for PU and PT-ZnO NPs, whereas for TE there is a change in the slope at high frequencies. In the commercial coatings after 720 h, the impedance modulus [Z] at 0.1 Hz was 1.09 × 10^{10}, 3.00 × 10^9, and 1.82 × 10^8 Ω cm^2 for PU, TE, and PT-ZnO NPs, respectively. This behavior presented in the evaluated coatings indicates that the electrolyte solution slowly penetrated the coatings (PU, TE, and PT-ZnO NPs). This resulted in the narrowing of the frequency range exhibiting capacitive behavior (PU, TE) in the Bode Phase diagram. The maximum phase angle shifted to higher frequencies (90–120°), but in the case of PT-ZnO NPs, the behavior is resistive.

All these indicate that the protective properties in the different commercial coating system decreased when there in an increase in the time of the prohesion tests. The decrease in resistance of the coatings is associated with the permeability of the chloride ions through the pores and the loss of the properties of the top layer in all the coatings evaluated. Prolonged exposure to ultraviolet light decreases the physical barrier effect generated by the top coat. The loss of the physical barrier generated by the top layer allows the migration of chloride ions from the primer to the metal substrate, causing an interaction or initiation of corrosion on the substrate. In this sense, it is possible that the barrier effect of the film is being partially lost due to the degradation of the coatings in certain areas, allowing direct contact between the metal and the evaluation environment. The decrease in the value of the impedance module to values between 10^{10} and 10^9 Ω cm^2 in commercial coatings indicates the beginning of the corrosion process. This process occurs at the substrate/paint interface in the defective areas of the coating, specifically in the process of charge transfer between the metal and the solution. The results indicate that the aggressive agent reached the substrate/coating interface, initiating a corrosive process in the steel. However, in the PT-ZnO NPs coating, a decrease in the impedance module is not observed since the tannins form iron tannates that protect the metallic substrate, thus preventing contact with the medium. After 720 h, PU coating exhibits a higher resistance to the aggressive agent when compared to PT-ZnO NPs and TE. The most affected coating is the TE, presenting a smaller

semicircle diameter compared to the PU and PT-ZnO NPs systems [50–52]. Table 5 shows the impedance modulus at the initial condition and 720 h.

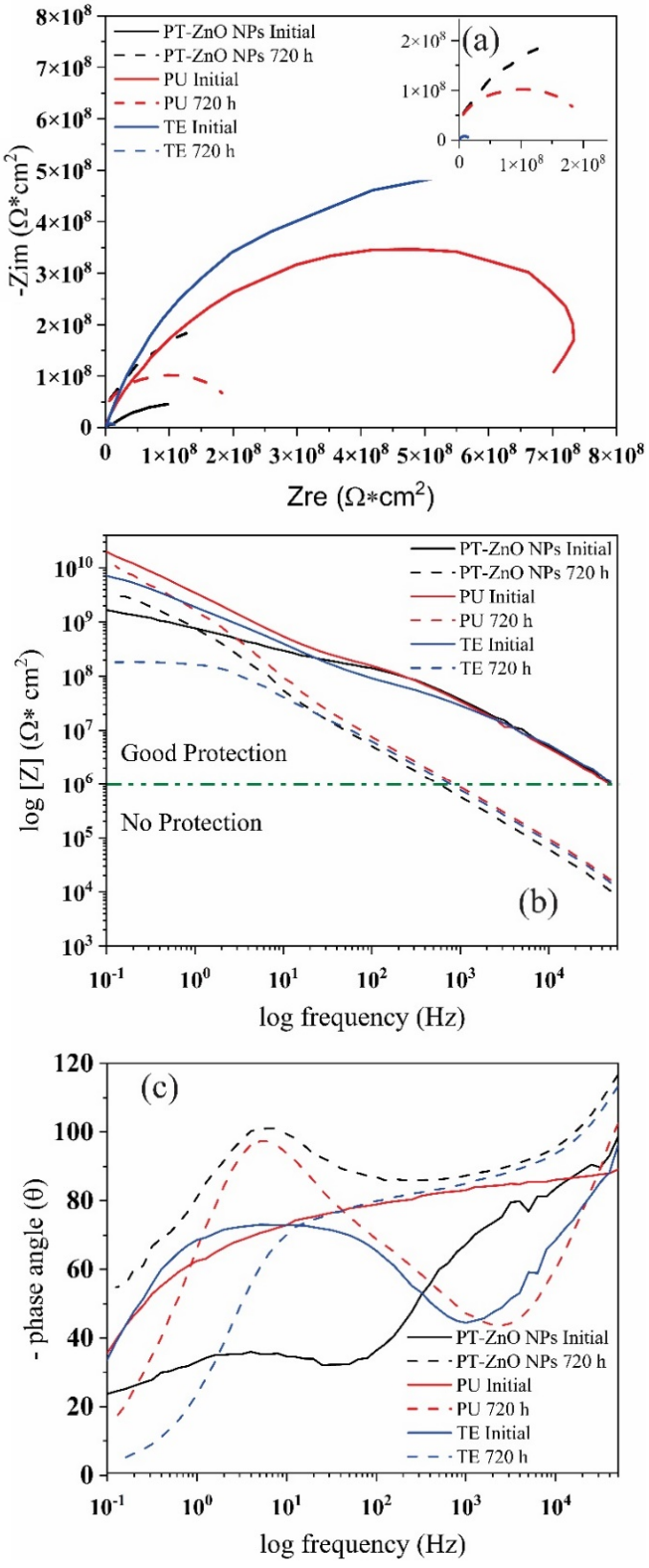

Figure 11. Nyquist and Bode phase diagrams for the coatings exposed to accelerated tests (**a**) Nyquist, (**b**) Bode modulus, and (**c**) Bode angle.

Table 5. Impedance modulus in the coatings exposed to accelerated tests.

Coatings	Time (h)	Z [Ω/cm^2]
PT-ZnO NPs	0	2.36×10^9
	720	3.00×10^9
PU	0	6.40×10^{10}
	720	1.04×10^{10}
TE	0	8.98×10^9
	720	1.82×10^8

Coating Exposed in the Field

Figure 12 shows the Nyquist and Bode diagrams of the coatings exposed to field tests. At time 0 h, all the coatings exhibited the formation of an incomplete resistive semicircles or loop with higher diameters and a one-time constant (Figure 12a). The modulus of the Bode plot exhibits a change in the slope at high and low frequencies for PU, TE, and PT-ZnO NPs (Figure 12b). On the other hand, in Figure 12b, the Bode diagram log frequency versus the phase for the analyzed coatings, there exists one-time constants and the corresponding phase angle is 90 degrees, thus causing it to behave similar to an ideal capacitor [53,54]. The impedance modulus [Z] at 0.1 Hz exhibited by the commercial PU coating was 5.50×10^{10} Ω cm^2 when compared to TE and PT-ZnO NPs with 6.70×10^9 Ω cm^2 and 3.51×10^9 Ω cm^2, respectively. In this sense, the impedance modulus [Z] at 0.1 Hz value presented by the coatings is greater than 1×10^8 Ω cm^2, implying that there is an excellent protective layer of the metallic substrate against aggressive agents [42,55].

After four months of exposure, the Nyquist plot exhibit the same formation of an incomplete resistive semicircle or loop on all exposed coatings, but with a higher diameter and the presence of a one-time constant. This result implies that the exposure medium is not as aggressive because the physical barrier established by the top layer limits the entry of the aggressive agent (sea salt spray and UV radiation) [46,47,53]. In addition, a higher semicircle diameter results in a high resistance of the coatings. Based on the results, there are no reactions in the interface area since there is no permeability of the aggressive agent through the pores. There is also no loss of the properties of the top coat. In this sense, the top layer enabled protection against the aggressive agent and the ultraviolet light, which did not deteriorate the physical barrier, thus the migration of chloride ions from the primer to the metal substrate is not expected. Due to this, there is no possibility of corrosion in the substrate. This is also verified by not observing the formation of another semicircle in the Nyquist diagram. According to the result, the coating scheme that presents a greater resistance to the aggressive agent after 4 months corresponds to the PU coating when compared to PT-ZnO NPs and TE. The coating with a smaller semicircle diameter corresponds to PT-ZnO NPs when compared to that of PU and TE systems [54].

In this sense, there is no permeation of the aggressive agent (chloride ions) through the pores of the coating to the surface of the metal substrate, so redox reactions (corrosion) could not be generated. In addition, this indicates that the top coat has good barrier properties and no degradation. After the exposure time, the impedance modulus of the evaluated coatings increased slightly, with an average of 10^9 Ω cm^2. The highest impedance [Z] at 0.1 after four months of exposure was presented by the commercial PU coating with 1.30×10^{10} Ω cm^2 when compared to TE and PT-NPs ZnO with 4.94×10^9 Ω cm^2 and 6.70×10^8 Ω cm^2, respectively. According to the [Z] at 0.1 of EIS in the evaluated coatings, the metallic substrate is protected since the modulus is greater than 10^6 Ω cm^2. This is confirmed in the angle Bode plot, which exhibits no variation in the angles nor the formation of a second time constant (Figure 12c). This behavior indicates that a corrosion process does not exist in the evaluated coatings (PT-ZnO NPs, PU, and TE) after 4 months of exposure in the field. Table 6 shows the impedance modulus at the initial condition and 4 months.

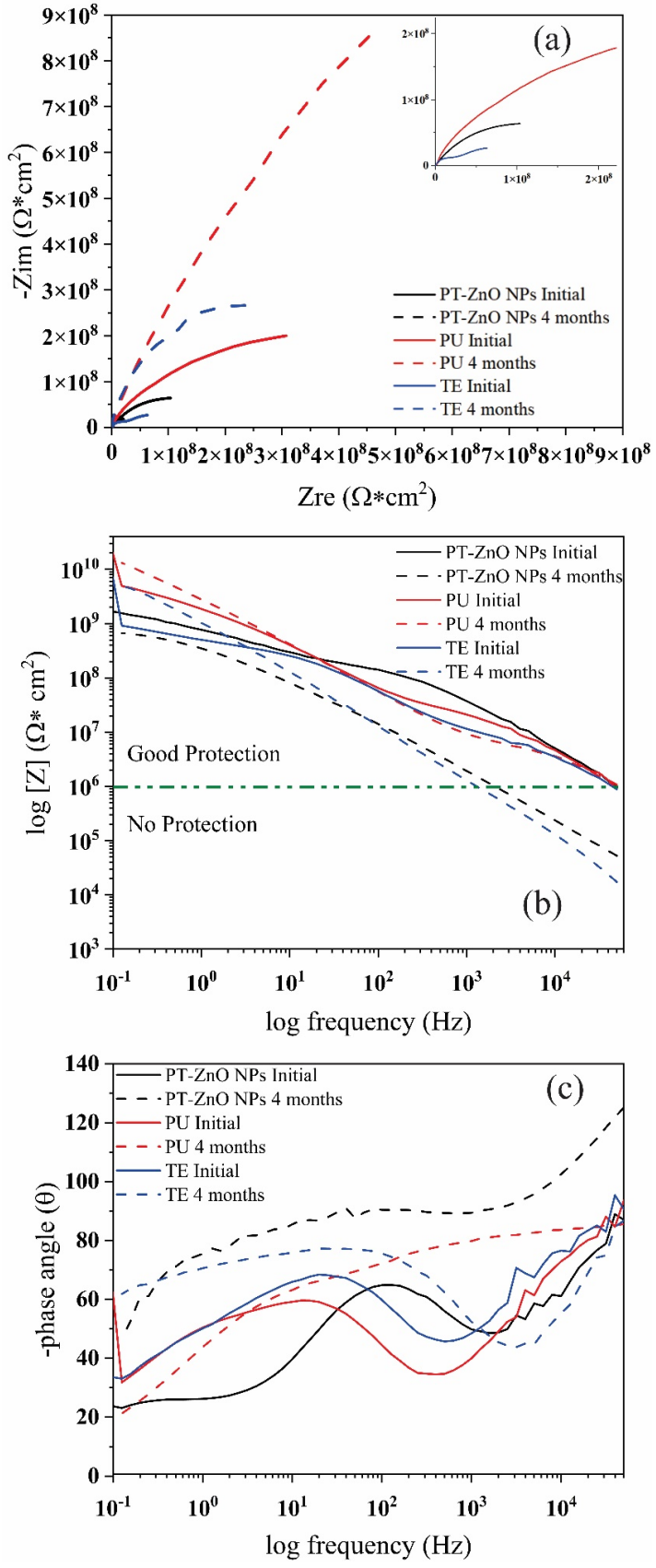

Figure 12. Nyquist and Bode phase diagrams for the coatings exposed in the fields: (**a**) Nyquist, (**b**) Bode modulus, and (**c**) Bode angle.

Table 6. Impedance modulus exposed in the field.

Coatings	Time (Months)	Z [Ω/cm^2]
PT-ZnO NPs	0	3.51×10^9
	4	6.70×10^8
PU	0	5.50×10^{10}
	4	1.30×10^{10}
TE	0	6.70×10^9
	4	5.19×10^8

4. Conclusions

The present work investigates the evaluation in real conditions of new anticorrosive formulations based on polyphenols from natural sources and encapsulated nanoparticles. For this purpose, the coatings were submitted to a prohesion test and field tests. The aggressive atmosphere of the city of Talcahuano (Talcahuano Maritime Government) was classified as C3 (medium aggressive) according to the metereochemical factors (Cl^-, SO_2, and TOW) applied in the ISO 9223 standard. The film properties of the evaluated schemes exhibited reduced film thickness and brightness after exposure to prohesion tests (720 h) and field tests (4 months). TE was the most affected coating with a higher loss in thickness (30%), blistering defects (2S2), and delamination (3S2) compared to PT-ZnO NPs and PU according to the ISO-4628 standard. The results of the mechanical properties confirm that the formulated PT-ZnO NPs coating has similar or superior properties to the commercial coatings (PU and TE) except for impact resistance when compared to TE. The prohesion test had an influence on the adhesion results, whose coatings presented mainly adhesive failure after exposing the samples at 720 h. The adhesion results show that the PT-ZnO NPs and PU coatings had decreased adhesion at values of 12.28 and 12.08 MPa when compared with TE (4.55 MPa). The results obtained from electrochemical impedance spectroscopy in the prohesion tests and field tests exhibit good behavior: the results showed that after 720 h the impedance modulus [Z] at 0.1 Hz was 1.09×10^{10} Ω cm^2, 3.00×10^2 Ω cm^2, and 1.82×10^8 Ω cm^2 for PU, TE, and PT-ZnO NPs, after four months of exposure the impedance modulus [Z] at 0.1 Hz of PU coating was 1.30×10^{10} Ω cm^2 when compared to TE and PT-NPs ZnO with 4.94×10^9 Ω cm^2 and 6.70×10^8 Ω cm^2, respectively. According to the [Z] at 0.1 of EIS in the evaluated coatings, the metallic substrate is protected since the modulus is greater than 10^6 Ω cm^2. This behavior in the evaluated PT-ZnO NPs coatings indicates high resistance against the aggressive agent. Finally, the content of tannins and ZnO NPs increases the functionality properties (film, mechanical, and corrosion).

Author Contributions: A.D.-G. and S.S.S. carried out the tannin extraction and its complete characterization. J.R., A.F.J. and Á.O. designed the experiments. L.F.M. and A.F.J. carried out the coating characterization. M.F.M. and D.R. analyzed the results and wrote the manuscript. A.D.-G. and J.R. developed the field tests and consolidated the formulations obtained. All the authors reviewed the manuscript and contributed to its consolidation. All authors have read and agreed to the published version of the manuscript.

Funding: This work was funded by National Agency for Research and Development of Chile (ANID), projects: FONDEQUIP N°EQM150139, PIA/APOYO CCTE AFB170007, FONDECYT Initiation 11190358, Fondef IT21I0006.

Institutional Review Board Statement: Not applicable.

Informed Consent Statement: Not applicable.

Data Availability Statement: Not applicable.

Acknowledgments: The authors would like to thank to the Interdisciplinary Group of Advanced Nanocomposites (Grupo Interdisciplinario de Nanocompuestos Avanzados, GINA) of the Department of Engineering Materials (DIMAT, according to its Spanish acronym), Engineering School of the University of Concepción, for its laboratory of nanospectroscopy (LAB-NANOSPECT). M.F.M. would like to thank Valentina Lamilla and Juliana Meléndrez for her enormous support.

Conflicts of Interest: The authors declare no conflict of interest.

References

1. Soares, C.G.; Garbatov, Y.; Zayed, A.; Wang, G. Influence of environmental factors on corrosion of ship structures in marine atmosphere. *Corros. Sci.* **2009**, *51*, 2014–2026. [CrossRef]
2. Morcillo, M.; Alcántara, J.; Díaz, I.; Chico, B.; Simancas, J.; De la Fuente, D. Marine atmospheric corrosion of carbon steels. *Rev. Metal.* **2015**, *51*, e045. [CrossRef]
3. De la Fuente, D.; Díaz, I.; Simancas, J.; Chico, B.; Morcillo, M. Long-term atmospheric corrosion of mild steel. *Corros. Sci.* **2011**, *53*, 604–617. [CrossRef]
4. Morcillo, M.; Chico, B.; Díaz, I.; Cano, H.; de la Fuente, D. Atmospheric corrosion data of weathering steels. A review. *Corros. Sci.* **2013**, *77*, 6–24. [CrossRef]
5. Palraj, S.; Selvaraj, M.; Maruthan, K.; Natesan, M. Kinetics of atmospheric corrosion of mild steel in marine and rural environments. *J. Mar. Sci. Appl.* **2015**, *14*, 105–112. [CrossRef]
6. Vera, R.; Delgado, D.; Rosales, B.M. Effect of atmospheric pollutants on the corrosion of high power electrical conductors—Part 2. Pure copper. *Corros. Sci.* **2007**, *49*, 2329–2350. [CrossRef]
7. De la Fuente, D.; Díaz, I.; Alcántara, J.; Chico, B.; Simancas, J.; Llorente, I.; García-Delgado, A.; Jiménez, J.A.; Adeva, P.; Morcillo, M. Corrosion mechanisms of mild steel in chloride-rich atmospheres. *Mater. Corros.* **2016**, *67*, 227–238. [CrossRef]
8. Amalvy, J.I.; Aznar, A.C.; Pardini, O.R.; Guzmán, G.A. Waterborne Anticorrosive Systems for Steel Protection—Part 1: Formulation and Testing. *Corrosion* **2002**, *58*, 871–880. [CrossRef]
9. Montemor, M.F. Functional and smart coatings for corrosion protection: A review of recent advances. *Surf. Coat. Technol.* **2014**, *258*, 17–37. [CrossRef]
10. Riaz, U.; Nwaoha, C.; Ashraf, S.M. Recent advances in corrosion protective composite coatings based on conducting polymers and natural resource derived polymers. *Prog. Org. Coat.* **2014**, *77*, 743–756. [CrossRef]
11. Akram, D.; Sharmin, E.; Ahmad, S. Synthesis, characterization and corrosion protective properties of boron-modified polyurethane from natural polyol. *Prog. Org. Coat.* **2008**, *63*, 25–32. [CrossRef]
12. Rani, B.E.A.; Basu, B.B.J. Green Inhibitors for Corrosion Protection of Metals and Alloys: An Overview. *Int. J. Corros.* **2012**, *2012*, 380217. [CrossRef]
13. Twite, R.L.; Bierwagen, G.P. Review of alternatives to chromate for corrosion protection of aluminum aerospace alloys. *Prog. Org. Coat.* **1998**, *33*, 91–100. [CrossRef]
14. Lamaka, S.V.; Zheludkevich, M.L.; Yasakau, K.A.; Montemor, M.F.; Ferreira, M.G.S. High effective organic corrosion inhibitors for 2024 aluminium alloy. *Electrochim. Acta* **2007**, *52*, 7231–7247. [CrossRef]
15. Eugene, U.; O'Donnell, P.S.; Ifeoma, V.J.; Feyisayo, V.A. The effect of corrosion inhibitors on stainless steels and aluminium alloys: A review. *African J. Pure Appl. Chem.* **2016**, *10*, 23–32. [CrossRef]
16. Mukherjee, A.; Joshi, M.; Misra, S.C.; Ramesh, U.S. Antifouling paint schemes for green SHIPS. *Ocean Eng.* **2019**, *173*, 227–234. [CrossRef]
17. Montoya, L.F.; Contreras, D.; Jaramillo, A.F.; Carrasco, C.; Fernández, K.; Schwederski, B.; Rojas, D.; Melendrez, M.F. Study of anticorrosive coatings based on high and low molecular weight polyphenols extracted from the Pine radiata bark. *Prog. Org. Coat.* **2019**, *127*, 100–109. [CrossRef]
18. LeBozec, N.; Thierry, D.; Le Calvé, P.; Favennec, C.; Pautasso, J.-P.; Hubert, C. Performance of marine and offshore paint systems: Correlation of accelerated corrosion tests and field exposure on operating ships. *Mater. Corros.* **2015**, *66*, 215–225. [CrossRef]
19. Jaramillo, A.F.; Montoya, L.F.; Prabhakar, J.M.; Sanhueza, J.P.; Fernández, K.; Rohwerder, M.; Rojas, D.; Montalba, C.; Melendrez, M.F. Formulation of a multifunctional coating based on polyphenols extracted from the Pine radiata bark and functionalized zinc oxide nanoparticles: Evaluation of hydrophobic and anticorrosive properties. *Prog. Org. Coat.* **2019**, *135*, 191–204. [CrossRef]
20. Selvakumar, N.; Jeyasubramanian, K.; Sharmila, R. Smart coating for corrosion protection by adopting nano particles. *Prog. Org. Coat.* **2012**, *74*, 461–469. [CrossRef]
21. Ramezanzadeh, B.; Attar, M.M. Studying the corrosion resistance and hydrolytic degradation of an epoxy coating containing ZnO nanoparticles. *Mater. Chem. Phys.* **2011**, *130*, 1208–1219. [CrossRef]
22. Noor Idora, M.S.; Ferry, M.; Wan Nik, W.B.; Jasnizat, S. Evaluation of tannin from Rhizophora apiculata as natural antifouling agents in epoxy paint for marine application. *Prog. Org. Coat.* **2015**, *81*, 125–131. [CrossRef]
23. Mansour, E.M.E.; Abdel-Gaber, A.M.; Abd-El Nabey, B.A.; Khalil, N.; Khamis, E.; Tadros, A.; Aglan, H.; Ludwick, A. Developing and Testing of a New Anticorrosive Coating Containing Algae as a Natural Inhibitor for Preventing Marine Corrosion of Steel. *Corrosion* **2003**, *59*, 242–249. [CrossRef]

24. Rosales, B.M.; Di, A.R.; De Rincón, O.; Rincón, A.; Elsner, C.I.; Marchisio, B. An evaluation of coil coating formulations in marine environments. *Prog. Org. Coat.* **2004**, *50*, 105–114. [CrossRef]
25. Elsner, C.I.; Cavalcanti, E.; Ferraz, O.; Di Sarli, A.R. Evaluation of the surface treatment effect on the anticorrosive performance of paint systems on steel. *Prog. Org. Coat.* **2003**, *48*, 50–62. [CrossRef]
26. Schmidt, D.P.; Shaw, B.A.; Sikora, E.; Shaw, W.W.; Laliberte, L.H. Corrosion protection assessment of sacrificial coating systems as a function of exposure time in a marine environment. *Prog. Org. Coat.* **2006**, *57*, 352–364. [CrossRef]
27. Medina, M.C.; Rojas, D.; Flores, P.; Peréz-Tijerina, E.; Meléndrez, M.F. Effect of ZnO nanoparticles obtained by arc discharge on thermo-mechanical properties of matrix thermoset nanocomposites. *J. Appl. Polym. Sci.* **2016**, *133*, 1–8. [CrossRef]
28. Jaramillo, A.F.; Baez-Cruz, R.; Montoya, L.F.; Medinam, C.; Pérez-Tijerina, E.; Salazar, F.; Rojas, D.; Melendrez, M.F. Estimation of the surface interaction mechanism of ZnO nanoparticles modified with organosilane groups by Raman Spectroscopy. *Ceram. Int.* **2017**, *43*, 11838–11847. [CrossRef]
29. Solis-Pomar, F.; Jaramillo, A.; Lopez-Villareal, J.; Medina, C.; Rojas, D.; Mera, A.C.; Meléndrez, M.F.; Pérez-Tijerina, E. Rapid synthesis and photocatalytic activity of ZnO nanowires obtained through microwave-assisted thermal decomposition. *Ceram. Int.* **2016**, *42*, 18045–18052. [CrossRef]
30. Mostafaei, A.; Zolriasatein, A. Synthesis and characterization of conducting polyaniline nanocomposites containing ZnO nanorods. *Prog. Nat. Sci. Mater. Int.* **2012**, *22*, 273–280. [CrossRef]
31. Martínez, C.; Briones, F.; Villarroel, M.; Vera, R. Effect of atmospheric corrosion on the mechanical properties of SAE 1020 structural steel. *Materials* **2018**, *11*, 591. [CrossRef]
32. Valverde, B.; Vera, R.; Henríquez, N.; Olave, E. Evaluation of atmospheric galvanic aluminum corrosion in electrical transmission towers at different sites in the Valparaíso region, Chile. Wire-on-Bolt Test (CLIMAT). *Mater. Corros.* **2021**, *72*, 1607–1619. [CrossRef]
33. Vera, R.; Araya, R.; Garín, C.; Ossandón, S.; Rojas, P. Study on the effect of atmospheric corrosion on mechanical properties with impact test: Carbon steel and Galvanized steel. *Mater. Corros.* **2019**, *70*, 1151–1161. [CrossRef]
34. De la Fuente, D.; Alcántara, J.; Chico, B.; Díaz, I.; Jiménez, J.A.; Morcillo, M. Characterisation of rust surfaces formed on mild steel exposed to marine atmospheres using XRD and SEM/Micro-Raman techniques. *Corros. Sci.* **2016**, *110*, 253–264. [CrossRef]
35. Ismail, E.A.; Motawie, A.M.; Sadek, E.M. Synthesis and characterization of polyurethane coatings based on soybean oil–polyester polyols. *Egypt. J. Pet.* **2011**, *20*, 1–8. [CrossRef]
36. Sharmin, E.; Ashraf, S.M.; Ahmad, S. Synthesis, characterization, antibacterial and corrosion protective properties of epoxies, epoxy-polyols and epoxy-polyurethane coatings from linseed and Pongamia glabra seed oils. *Int. J. Biol. Macromol.* **2007**, *40*, 407–422. [CrossRef]
37. Nnaji, N.J.N.; Okoye, C.O.B.; Obi-Egbedi, N.O.; Ezeokonkwo, M.A.; Ani, J.U. Spectroscopic characterization of red onion skin tannin and it's use as alternative aluminium corrosion inhibitor in hydrochloric acid solutions. *Int. J. Electrochem. Sci.* **2013**, *8*, 1735–1758.
38. Velayutham, T.S.; Majid, W.H.A.; Ahmad, A.B.; Kang, G.Y.; Gan, S.N. Synthesis and characterization of polyurethane coatings derived from polyols synthesized with glycerol, phthalic anhydride and oleic acid. *Prog. Org. Coat.* **2009**, *66*, 367–371. [CrossRef]
39. Yu, D.; Wang, J.; Tian, J.; Xu, X.; Dai, J.; Wang, X. Preparation and characterization of TiO2/ZnO composite coating on carbon steel surface and its anticorrosive behavior in seawater. *Compos. Part B Eng.* **2013**, *46*, 135–144. [CrossRef]
40. Olad, A.; Nosrati, R. Preparation and corrosion resistance of nanostructured PVC/ZnO-polyaniline hybrid coating. *Prog. Org. Coat.* **2013**, *76*, 113–118. [CrossRef]
41. Palraj, S.; Selvaraj, M.; Maruthan, K.; Rajagopal, G. Corrosion and wear resistance behavior of nano-silica epoxy composite coatings. *Prog. Org. Coat.* **2015**, *81*, 132–139. [CrossRef]
42. Sørensen, P.A.; Kiil, S.; Dam-Johansen, K.; Weinell, C.E. Anticorrosive coatings: A review. *J. Coat. Technol. Res.* **2009**, *6*, 135–176. [CrossRef]
43. Mostafaei, A.; Nasirpouri, F. Epoxy/polyaniline–ZnO nanorods hybrid nanocomposite coatings: Synthesis, characterization and corrosion protection performance of conducting paints. *Prog. Org. Coat.* **2014**, *77*, 146–159. [CrossRef]
44. Matamala, G.; Smeltzer, W.; Droguett, G. Use of Tannin Anticorrosive Reaction Primer to Improve Traditional Coating Systems. *Corrosion* **1994**, *50*, 270–275. [CrossRef]
45. Bakhshandeh, E.; Jannesari, A.; Ranjbar, Z.; Sobhani, S.; Saeb, M.R. Anti-corrosion hybrid coatings based on epoxy–silica nano-composites: Toward relationship between the morphology and EIS data. *Prog. Org. Coat.* **2014**, *77*, 1169–1183. [CrossRef]
46. Vivier, V.; Orazem, M.E. Impedance Analysis of Electrochemical Systems. *Chem. Rev.* **2022**, *122*, 11131–11168. [CrossRef]
47. Yu, F.; Dai, X.; Beebe, T.; Hsiai, T. Electrochemical impedance spectroscopy to characterize inflammatory atherosclerotic plaques. *Biosens. Bioelectron.* **2011**, *30*, 165–173. [CrossRef]
48. Bastidas, D.M. Interpretation of impedance data for porous electrodes and diffusion processes. *Corrosion* **2007**, *63*, 515–521. [CrossRef]
49. Lasia, A. Electrochemical Impedance Spectroscopy and its Applications. *Mod. Asp. Electrochem.* **1999**, *32*, 143–248. [CrossRef]
50. Park, S.-M.; Yoo, J.-S.; Chang, B.-Y.; Ahn, E.-S. Novel instrumentation in electrochemical impedance spectroscopy and a full description of an electrochemical system. *Pure Appl. Chem.* **2006**, *78*, 1069–1080. [CrossRef]
51. Akbarinezhad, E.; Bahremandi, M.; Faridi, H.R.; Rezaei, F. Another approach for ranking and evaluating organic paint coatings via electrochemical impedance spectroscopy. *Corros. Sci.* **2009**, *51*, 356–363. [CrossRef]

52. Mansfeld, F.; Kendig, M.W.; Tsai, S. Evaluation of Corrosion Behavior of Coated Metals with AC Impedance Measurements. *Corrosion* **1982**, *38*, 478–485. [CrossRef]
53. O'Donoghue, M.; Garrett, R.; Datta, V.; Roberts, P.; Aben, T. EIS: Testing coatings for rapid immersion service. *Mater. Perform.* **2003**, *28*, 36–41.
54. Walter, G.W. The application of impedance spectroscopy to study the uptake of sodium chloride solution in painted metals. *Corros. Sci.* **1991**, *32*, 1041–1058. [CrossRef]
55. Alizadeh Razin, A.; Ramezanzadeh, B.; Yari, H. Detecting and estimating the extent of automotive coating delamination and damage indexes after stone chipping using electrochemical impedance spectroscopy. *Prog. Org. Coat.* **2016**, *92*, 95–109. [CrossRef]